

## Supporting Information

### Insight into the Effective Aerobic Oxidative Cross-Esterification of Alcohols over Au/Porous Boron Nitride Catalyst

Rong Zhang<sup>a,b,‡</sup>, Xi Yang<sup>a,c,‡</sup>, Zheng Tao<sup>a</sup>, Xiao Wang<sup>a</sup>, Huixiang Wang<sup>a</sup>, Liancheng Wang<sup>a,\*</sup>, Baoliang Lv<sup>a,\*</sup>

<sup>a</sup> *State Key Laboratory of Coal Conversion, Institute of Coal Chemistry, Chinese Academy of Sciences, Taiyuan, 030001, China*

<sup>b</sup> *University of Chinese Academy of Sciences, Beijing, 100049, China*

<sup>c</sup> *Department of Chemistry, Shanghai University, Shanghai 200444, China*

<sup>‡</sup> Rong Zhang and Xi Yang contributed to this manuscript equally.

\*Corresponding authors.

E-mail addresses: wanglc@sxicc.ac.cn, lbl604@sxicc.ac.cn.

#### Table of Contents

S1. Electrochemical measurements

Table S1. The specific surface area and pore volume of the catalysts.

Figure S1. TEM images of Au/*p*BN, Au/BN<sub>c</sub>.

Figure S2. The XRD pattern Au/BN<sub>c</sub>.

Figure S3. XPS spectra of Au/*p*BN catalyst, C1s, O1s.

Figure S4. The catalytic performance of Au/BN<sub>c</sub> catalyst.

Figure S5. The oxidative esterification performance of 20 mg Au/*p*BN catalyst (1/5 of

the original amount).

Figure S6. The TPD profiles of methanol and benzyl alcohol on Au/BN<sub>c</sub>.

Figure S7. The FT-IR spectrum of pure *p*BN after annealing at 300°C.

Figure S8. Cycles of the oxidative esterification over Au/*p*BN catalyst.

Figure S9. The TEM images of the used Au/*p*BN catalyst.

## S1. Electrochemical measurements

**Preparation of Working Electrode.** A catalyst ink was made by ultrasonically dispersing 5 mg catalyst in 1 mL of ethanol and Nafion (DuPont, 5 wt.%, 8:2 Vol/Vol) mixture to form homogeneous suspension. Then, the ink of 10  $\mu\text{L}$  was dispersed onto a glassy carbon rotating disk electrode (RDE, 5 mm diameter, Pine Instrument Co.Ltd. USA) and dried thoroughly under ambient atmosphere for 12 h.

**Cyclic Voltammetry.** Cyclic voltammetry (CV) analyses and electrocatalysis of the catalysts were conducted using an electrochemical workstation (CHI 760D, CH Instruments, Inc., Shanghai, China) and rotating disk electrode system (RDE, 5 mm diameter, Pine Instrument Co.Ltd. USA). And a three-electrode configuration was employed, which consisting of an Ag/AgCl as the reference electrode (KOH, 3 M), a platinum wire as the counter electrode and the glassy carbon rotating ring-disk electrode loading with catalysts as the working electrode. The cyclic voltammetry was performed in 0.1 M  $\text{K}_2\text{CO}_3$  solution saturated with oxygen ( $\text{O}_2$ ) or nitrogen ( $\text{N}_2$ ) at a scan rate of  $50 \text{ mV}\cdot\text{s}^{-1}$ . RDE voltammetry was carried out in  $\text{O}_2$ -saturated 0.1 M  $\text{K}_2\text{CO}_3$  solution at a scanning rate of  $10 \text{ mV}\cdot\text{s}^{-1}$  with various rotation rates (400–2500 rpm).

All the potentials in this work were converted to the reference of the reversible hydrogen electrode (RHE) according to the following equation:

$$E_{(\text{RHE})} = E_{(\text{Ag}/\text{AgCl})} + E_{\text{Ag}/\text{AgCl}}^{\theta} + 0.059\text{pH}.$$

Table S1. Details of specific surface area and pore volume of the catalysts.

Sample	$S_{\text{BET}}$ ( $\text{m}^2 \cdot \text{g}^{-1}$ )	$S_{\text{micropore}}$ ( $\text{m}^2 \cdot \text{g}^{-1}$ )	External Surface Area	$V_{\text{micropore}}$ ( $\text{cm}^3 \cdot \text{g}^{-1}$ )	$V_{\text{total}}$ ( $\text{cm}^3 \cdot \text{g}^{-1}$ )
<i>p</i> BN	281.0	64.1	216.9	0.027	0.69
Au/ <i>p</i> BN	256.7	52.0	204.8	0.022	0.73
Au/BN <sub>c</sub>	26.4	/	/	/	/
Used Au/ <i>p</i> BN	204.2	44.2	160.0	0.020	0.56

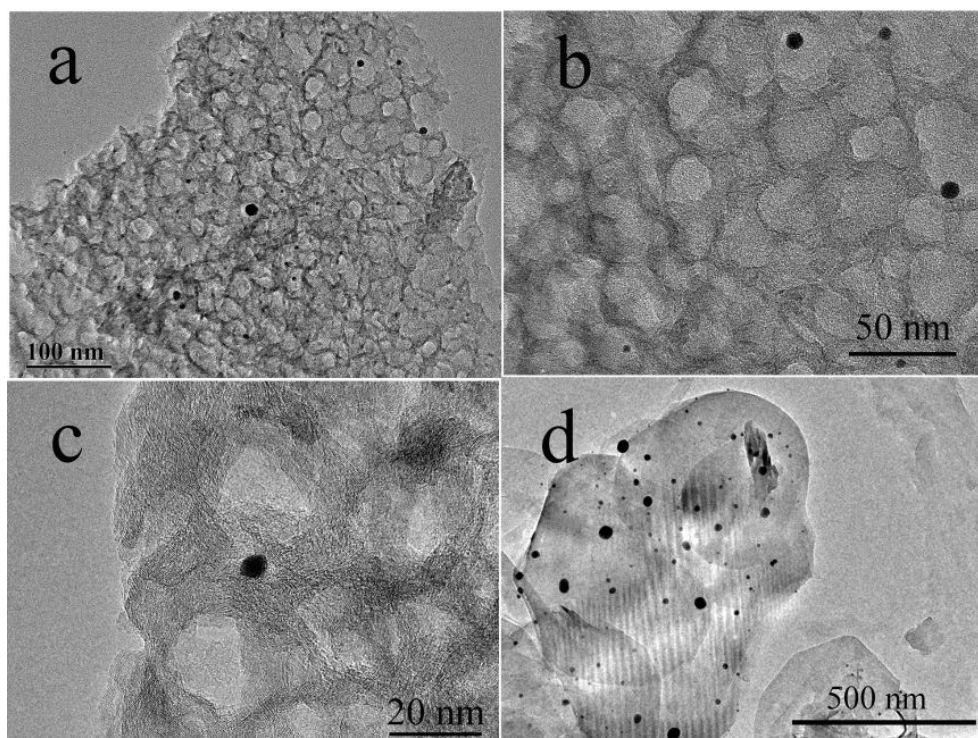


Figure S1. The TEM images ( a, b overview, c enlarged view) of the Au/*p*BN and (d) Au/BN<sub>c</sub> catalyst.

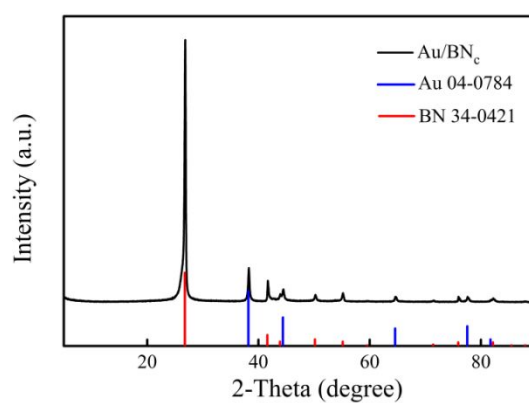


Figure S2. The XRD pattern of Au/BN<sub>c</sub> catalyst.

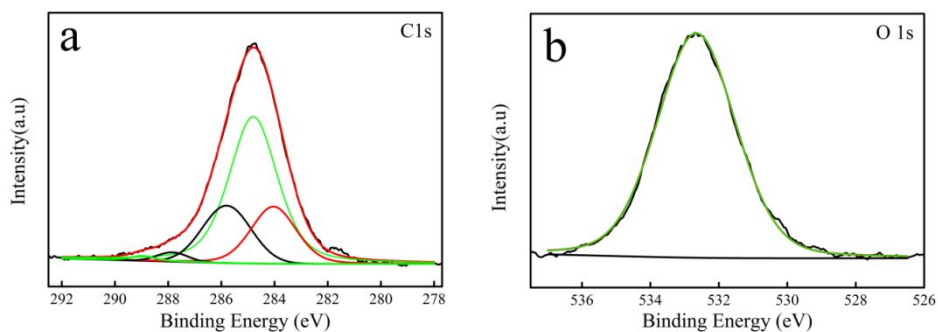


Figure S3. XPS spectra of Au/pBN catalyst, C1s(a), O1s(b).

The main peak at 284.6 eV corresponds to the C=C bonding in graphite, indicating the presence of the graphitic domains within the B-N network. The shoulder peaks at 284.0 and 285.8 eV could belong to the C-B, and C-N bonding, respectively, indicating the existence of boundaries between the *h*-BN and graphitic regions. The shoulder peaks at 287.9 and 288.9 eV corresponds to C-O and -C=O bonding, respectively. The presence of oxygen was probably due to the surface oxygen-containing groups and the physicochemically adsorbed oxygen-containing components, O<sub>2</sub> and CO<sub>2</sub>.

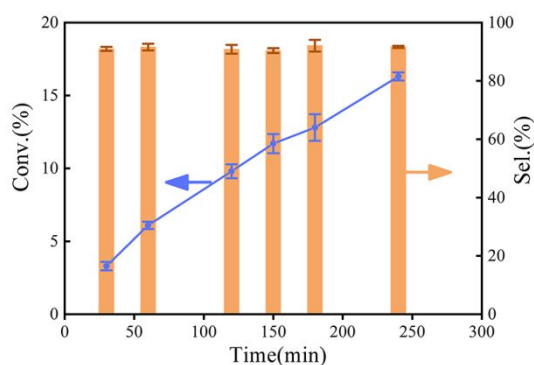


Figure S4. The catalytic performance of Au/BN<sub>c</sub> catalyst; Reaction condition: 98 mg catalyst, 2.5 mmol benzyl alcohol, 8 ml methanol, 0.69 g K<sub>2</sub>CO<sub>3</sub>, P(O<sub>2</sub>)=0.1 MPa, T= 30 °C.

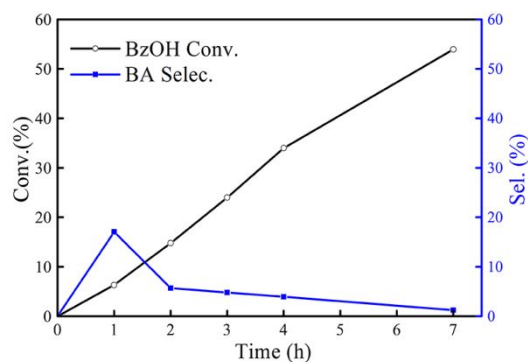


Figure S5. The conversion of BzOH and selectivity of BA vs. reaction time profiles with 20 mg Au/*p*BN catalyst, other experimental conditions are unchangeable.

To slow down the reaction rate, 1/5 of the original catalyst amount was used in the esterification reaction and the benzaldehyde (BA) intermediate was monitored. As shown in Figure S5, the BA can be later transformed to methyl benzoate (MB).

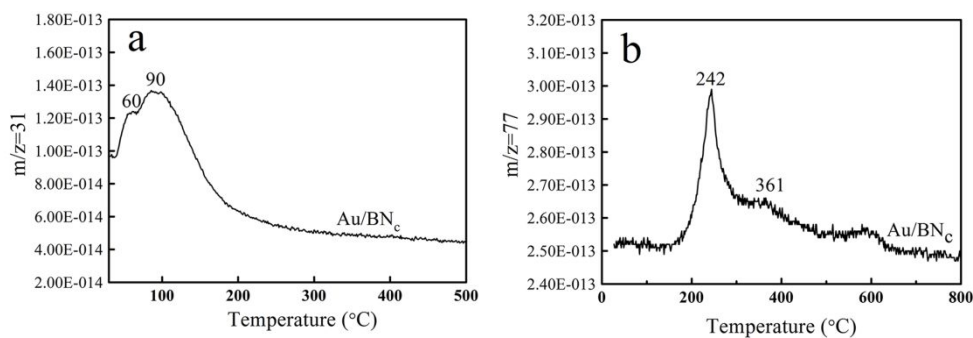


Figure S6. The TPD profiles of methanol (a) and benzyl alcohol (b) on Au/BN<sub>c</sub> catalyst under Ar atmosphere with a ramping rate of 10°C/min.

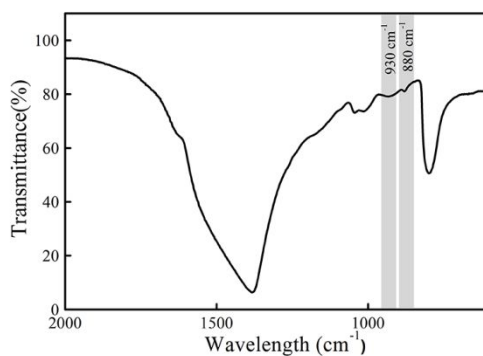


Figure S7. FT-IR spectrum of the pure *p*BN after annealing at 300 °C, the band at 930 cm<sup>-1</sup> can be attributed to the ν<sub>B-O-O-B</sub>.

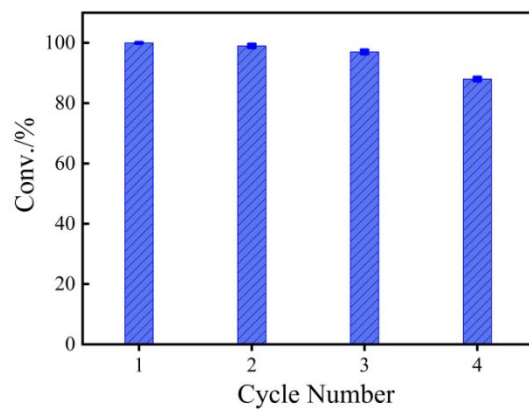


Figure S8. Cycles of the oxidative esterification reaction over the Au/pBN catalyst.

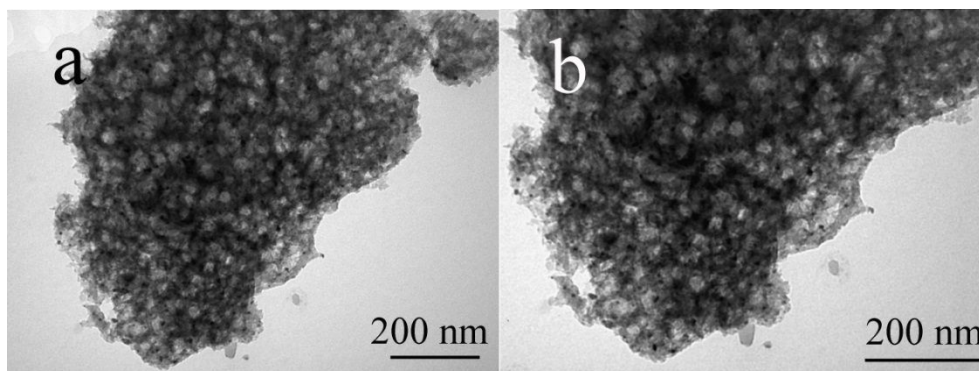


Figure S9. The TEM image (a) and higher-resolution image (b) of the used Au/pBN catalyst.